BIOCHEMISTRY
including biophysical chemistry & molecular biology
Article

Biochemistry **2010,** *49,* 3753–3765 3753
DOI: 10.1021/bi100187b

Kinetic Isotope Effects on the Noncovalent Flavin Mutant Protein of Pyranose 2-Oxidase Reveal Insights into the Flavin Reduction Mechanism†

Jeerus Sucharitakul,‡ Thanyaporn Wongnate,§ and Pimchai Chaiyen*,§

‡*Department of Biochemistry, Faculty of Dentistry, Chulalongkorn University, Henri-Dunant Road, Patumwan, Bangkok 10330, Thailand, and* §*Department of Biochemistry and Center of Excellence in Protein Structure and Function, Faculty of Science, Mahidol University, Bangkok 10400, Thailand*

Received February 6, 2010; Revised Manuscript Received March 31, 2010

ABSTRACT: Pyranose 2-oxidase (P2O) from *Trametes multicolor* contains a flavin adenine dinucleotide (FAD) cofactor covalently linked to the N^3 atom of His167. The enzyme catalyzes the oxidation of aldopyranoses by molecular oxygen to generate 2-keto-aldoses and H_2O_2 as products. In this study, the transient kinetics and primary and solvent kinetic isotope effects of the mutant in which His167 has been replaced with Ala (H167A) were investigated, to elucidate the functional role of the 8a-N^3-histidyl FAD linkage and to gain insights into the reaction mechanism of P2O. The results indicate that the covalent linkage is mainly important for a reductive half-reaction in which the FAD cofactor is reduced by D-glucose, while it is not important for an oxidative half-reaction in which oxygen reacts with the reduced FAD to generate H_2O_2. D-Glucose binds to H167A via multiple binding modes before the formation of the active Michaelis complex, and the rate constant of flavin reduction decreases ~22-fold compared to that of the wild-type enzyme. The reduction of H167A using D-glucose isotopes (2-*d*-D-glucose, 3-*d*-D-glucose, and 1,2,3,4,5,6,6-d_7-D-glucose) as substrates indicates that the primary isotope effect results only from substitution at the C2 position, implying that H167A catalyzes the oxidation of D-glucose regiospecifically at this position. No solvent kinetic isotope effect was detected during the reductive half-reaction of the wild-type or H167A enzyme, implying that the deprotonation of the D-glucose C2-OH group may occur readily upon the binding to P2O and is not synchronized with the cleavage of the D-glucose C2−H bond. The mutation has no drastic effect on the oxidative half-reaction of P2O, as H167A is very similar to the wild-type enzyme with respect to the kinetic constants and the formation of the C4a-hydroperoxyflavin intermediate. Kinetic mechanisms for both half-reactions of H167A were proposed on the basis of transient kinetic data and were verified by kinetic simulations and steady-state kinetic parameters.

Flavoenzymes containing covalent linkages are less common than flavoenzymes containing dissociable flavins. A large number of covalently linked flavoenzymes belong to the glucose-methanol-choline (GMC)[1] oxidoreductase and vanillyl-alcohol oxidoreductase families (*1*−*4*). The flavin linkages have been found as single linkages of C8α-N^1-histidyl, C8α-N^3-histidyl, C8α-*O*-tyrosyl, C8α-*S*-cysteinyl, C6-*S*-cysteinyl, or FMN-phosphoester-threonyl and bicovalent linkages of C8α-N^1-histidyl and C6-*S*-cysteinyl (*4*). Covalent flavinylation originates from an autocatalytic process in 6-hydroxy-D-nicotine oxidase (*2*), *p*-cresol methylhydroxylase (*5*), monomeric sarcosine oxidase (*6*), vanillyl-alcohol oxidase (VAO) (*7*), and trimethylamine dehydrogenase (*8*). The biochemical significance of the covalent flavin linkage varies among different enzymes and often includes increasing the redox potential for efficient catalysis, enhancing protein stability, and preventing chemical modification of the flavin cofactor during catalysis (*4*).

Pyranose 2-oxidase (P2O, pyranose:oxygen 2-oxidoreductase, EC 1.13.10) from *Trametes multicolor* is a member of the GMC oxidoreductase family. It catalyzes the oxidation of several aldopyranoses by molecular oxygen at the C2 position to yield the corresponding 2-keto-aldoses and hydrogen peroxide (*9*, *10*). The enzyme is useful for its application in sugar syntheses (*11*) and has recently been proposed for use in biofuel cell applications (*12*). P2O is a homotetrameric enzyme with a native molecular mass of 270 kDa (*9*). Each subunit contains one flavin adenine dinucleotide (FAD) that is covalently attached to N^3 of His167 (*13*). The catalytic reaction of P2O can be divided into a reductive half-reaction (in which two electrons are transferred as a hydride equivalent from a sugar substrate to generate reduced FAD and the corresponding 2-keto sugar) and an oxidative half-reaction (in which two electrons are transferred from the reduced flavin to oxygen to form hydrogen peroxide) (*14*, *15*). P2O is the

†This work was supported by The Thailand Research Fund through Grants BRG5180002 (to P.C.) and MRG4980117 (to J.S.) and by grants from the Faculty of Science, Mahidol University (to P.C.), from the Faculty of Dentistry, Chulalongkorn University (to J.S.), and from National Science and Technology Development Agency (to T.W.).

*To whom correspondence should be addressed: Department of Biochemistry and Center of Excellence in Protein Structure and Function, Faculty of Science, Mahidol University, Rama 6 Road, Bangkok 10400, Thailand. Telephone: 662-2015596. Fax: 662-3547174. E-mail: scpcy@mahidol.ac.th.

[1]Abbreviations: P2O, pyranose 2-oxidase; FAD, flavin adenine dinucleotide; H167A, mutant of P2O in which His167 has been replaced with Ala; WT, wild-type enzyme of P2O; k_{obs}, observed rate constant; KIE, kinetic isotope effect; SKIE, solvent kinetic isotope effect; G, D-glucose; 2FG, 2-fluorodeoxy-D-glucose; GMC, glucose-methanol-choline; VAO, vanillyl-alcohol oxidase; ABTS, 2,2′-azinobis(3-ethylbenzenethiazoline-6-sulfonic acid); E_{ox}, oxidized form of H167A; E_r, reduced form of H167A; E'_{ox}:G and E^*_{ox}:G, complexes of H167A and D-glucose; E''_{ox}:G and E^{**}_{ox}:G, isomerized complexes of H167A and D-glucose; E-C4a-OOH, C4a-hydroperoxy-FAD.

Published on Web 04/01/2010

first flavoprotein oxidase for which the formation of C4a-hydroperoxyflavin has been observed during the oxidative half-reaction (*15*). The C4a-flavin adduct was detected in other flavoprotein oxidases only under specific conditions such as in the crystalline form of choline oxidase (*16*) and the mutant form, C42S, of NADH oxidase (*17*). In addition, the reductive half-reaction of P2O has exhibited a few interesting features that are not found in other flavoprotein oxidases, such as an absorbance increase at 395 nm and an inverse kinetic isotope effect at the D-glucose binding step (*14*, *18*). The catalytic dehydrogenation of substrates containing hydroxyl groups by flavoprotein oxidases has been proposed to be initiated by the removal of the hydroxyl proton followed by the transfer of the hydride moiety (*19*). In many flavoprotein oxidases, solvent and primary kinetic isotope effects have been investigated to identify the relative timing between the deprotonation and hydride transfer steps (*19*, *20*). The mechanism of choline oxidase, a member of the GMC family, has been shown to occur stepwise (*21*, *22*). For P2O, no studies have investigated whether the deprotonation of the C2−OH group of D-glucose is synchronized with or decoupled from the hydride transfer.

The crystal structures of wild-type P2O (WT) and the H167A mutant in complex with a substrate analogue, 2-fluoro-2-deoxy-D-glucose (2FG), have been reported (*10*, *23*). The structure of H167A shows that 2FG binds in the orientation that is optimal for C3 oxidation (*23*). 2FG can reduce the wild-type enzyme more rapidly than H167A, preventing successful crystallization of the WT−2FG complex (*23*). The redox potential value of WT is −105 mV, and that of H167A is −150 mV (*23*). Comparing these values implies that the reduction of FAD in H167A by D-glucose should be slower than in WT. However, the transient kinetics of H167A has never been investigated. With the crystal structure available and the flavin−protein covalent linkage absent, this mutant serves as an ideal model for exploring the functional role of the *C8*α-N^3-histidyl−FAD linkage in enzyme catalysis. As the flavin reduction rate should be slower in H167A than in WT because of the decrease in the redox potential, the binding steps prior to the reduction step should be more resolved in the mutant than in WT.

In this study, we investigated the effects of the H167A mutation on both the reductive and oxidative half-reactions using transient kinetics. Reactions of H167A with 2-*d*-D-glucose, 3-*d*-D-glucose, and 1,2,3,4,5,6,6-d_7-D-glucose were conducted to identify the regiospecificity of the enzyme. Solvent kinetic isotope effects on the reactions of H167A and WT with D-glucose and 2-*d*-D-glucose were measured to explore the relative timing between the deprotonation of the C2−OH bond and the hydride transfer reaction from the C2−H group.

MATERIALS AND METHODS

Reagents. D-Glucose (99.5% pure) and horseradish peroxidase were purchased from Sigma-Aldrich Chemie GMG. Deuterated glucoses (2-*d*-D-glucose, 3-*d*-D-glucose, and 1,2,3,4,5,6,6-d_7-D-glucose), sodium deuteroxide (99%), and deuterium oxide (99.9%) were purchased from Cambridge Isotope Laboratory. ABTS [2,2′-azinobis(3)-ethylbenzenethiazoline-6-sulfonic acid diammonium salt] was purchased from Sigma-Aldrich. A non-covalent flavin mutant of P2O, H167A, was cloned, expressed, and prepared as previously described (*23*). This mutant was expressed in the absence of a His_6 tag to avoid its interfering properties. The concentrations of the following compounds were determined using the known extinction coefficients at pH 7.0: $\varepsilon_{403} = 1 \times 10^5\ M^{-1}\ cm^{-1}$ for peroxidase, $\varepsilon_{452} = 1.29 \times 10^4\ M^{-1}\ cm^{-1}$ for H167A, and $\varepsilon_{458} = 1.3 \times 10^4\ M^{-1}\ cm^{-1}$ for WT (*15*). These values assume one FAD bound per subunit.

Spectroscopic Studies. UV−visible absorbance spectra were recorded using a Hewlett-Packard diode array spectrophotometer (HP8453), a Shimadzu 2501PC spectrophotometer, or a Cary 300Bio double-beam spectrophotometer. All spectrophotometers were equipped with thermostated cell compartments. Enzyme activities were determined with a continuous assay using a coupled reaction of horseradish peroxidase and its substrate ABTS as previously described (*24*). Initial rates were calculated from the increase in absorbance at 420 nm resulting from the oxidation of ABTS by H_2O_2 using the molar absorption coefficient of $4.2 \times 10^5\ M^{-1}\ cm^{-1}$.

Determination of the Molar Absorption Coefficient of H167A. The mutant was denatured to separate FAD from the protein using TCA. In brief, a solution of H167A was diluted in 50 mM sodium phosphate buffer (pH 7.0) to yield a maximum absorbance at 450 nm of approximately 0.2 (1 mL) and precipitated using 5% TCA (*25*). The pH of the solution was adjusted to pH 7.0 using sodium carbonate (solid crystals), and the denatured protein was removed by centrifugation at 17400*g*. The concentration of the free FAD released from the denatured enzyme was determined on the basis of the free FAD molar absorption coefficient (ε_{450}) of $1.13 \times 10^4\ M^{-1}\ cm^{-1}$. The molar absorptivity of H167A (per FAD molecule) (ε_{452}) was calculated to be $1.29 \times 10^4\ M^{-1}\ cm^{-1}$.

Rapid Reaction Experiments. Reactions were conducted in 50 mM sodium phosphate buffer (pH 7.0) at 4 °C, unless otherwise specified. The measurements were performed using a Hi-Tech Scientific model SF-61DX stopped-flow spectrophotometer in single-mixing mode. The optical path length of the observation cell was 1 cm. The stopped-flow apparatus was made anaerobic by flushing the flow system with an anaerobic buffer solution containing 10 mM sodium dithionite in 50 mM sodium phosphate buffer (pH 7.0). The buffer for the sodium dithionite solution was made anaerobic by equilibration with oxygen-free nitrogen (ultrahigh purity) that had been passed through an Oxyclear oxygen removal column (Labclear). The anaerobic buffer was allowed to stand in the flow system overnight. The flow unit was then rinsed with the anaerobic buffer before the experiments. Apparent rate constants (k_{obs}) were calculated from the kinetic traces using exponential fits and the software packages Kinetic Studio (Hi-Tech Scientific, Salisbury, U.K.) and Program A [written at the University of Michigan (Ann Arbor, MI) by R. Chang, J. Chiu, J. Dinverno, and D. P. Ballou].

For the reduction of H167A by D-glucose or deuterated 2-*d*-D-glucose, a solution of the oxidized enzyme was placed in a tonometer and equilibrated with nitrogen before being loaded onto the stopped-flow machine. Then, a 3 mL solution of D-glucose at the desired concentration was placed in a 5 mL glass syringe and made anaerobic by being bubbled with oxygen-free nitrogen for 8 min before being loaded onto the stopped-flow machine. To study the reactions of the reduced enzyme with oxygen, an anaerobic enzyme solution was equilibrated in an anaerobic glovebox (Belle Technology) to control the concentration of oxygen at less than 3 ppm, and the enzyme was then reduced with a solution of D-glucose [~10 mM in 50 mM sodium phosphate buffer (pH 7.0)]. While a solution of D-glucose was being added, the enzyme spectra were recorded using a spectrophotometer inside the glovebox to ensure complete reduction. The reduced enzyme solution was placed in a glass tonometer and

Scheme 1

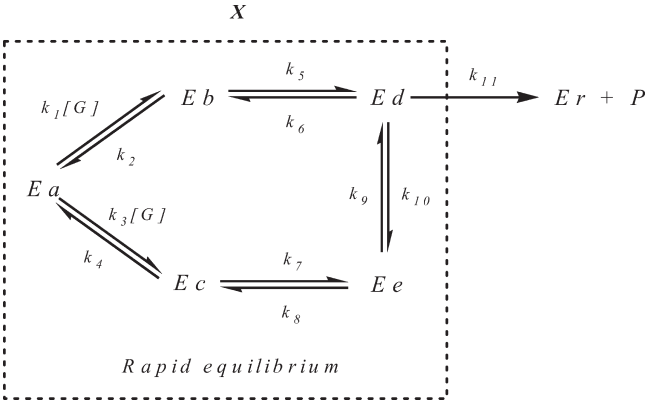

loaded onto the stopped-flow spectrophotometer. To study the solvent isotope effects on the kinetics of the flavin reduction, all solutions were exchanged into sodium phosphate buffer made with deuterium oxide. In brief, solid sodium phosphate powder (0.69 g) was dissolved in ~30 mL of 99.9% deuterium oxide, and the resulting solution was equilibrated for 13−15 h (overnight) in the anaerobic glovebox. The equilibrated solution was evaporated at 60 °C for 3 h using a rotary evaporator to yield H_2O-free sodium phosphate powder. The resulting powder was added to 99.9% deuterium oxide, and the same process was repeated to ensure that the buffer contained at least 99.9% deuterium oxide. The pD of the buffer was adjusted via addition of sodium deuteroxide to the solution while the pH was monitored (pD = $pH_{measured}$ + 0.4) (*26*). D-Glucose and 2-*d*-D-glucose were dissolved in ~20 mL of 99.9% deuterium oxide, and the solutions were dried twice, in a manner similar to the process described above. The resulting substrate powder was dissolved in 50 mM sodium phosphate buffer in deuterium oxide. Flavin reduction was monitored by following the absorbance at 400 and 452 nm. We created solutions with various concentrations of oxygen by bubbling certified oxygen/nitrogen gas mixtures through syringes. Rate constants were obtained from fits of k_{obs} versus the concentration of oxygen using Marquardt−Levenberg nonlinear fit algorithms included in KaleidaGraph (Synergy Software). Simulations were performed by numerical methods using Runge−Kutta algorithms implemented in Berkeley Madonna 8.3 and a time step of 3.125×10^{-4} s. The proposed model was created and used for simulations of the reductive and oxidative half-reactions.

Expression of the Observed versus Individual Rate Constants. A kinetic model for flavin reduction is shown in Scheme 1. The dotted line square defines the steps that are assumed to occur in the two pathways for rapid equilibrium binding of the substrate (G) to the enzyme (Ea), forming two forms of the enzyme−substrate complexes (Eb and Ec) that further convert to Ed and Ee, respectively. Only Ed is an active Michaelis complex that can be reduced by G. The relaxation times of all steps inside the square are much faster than the catalytic step (k_{11}).

According to Cha's method (*27*), all species in rapid equilibrium can be summed and represented as a simple term, X. This term represents all equilibrating fast enzyme forms. A rate constant for the conversion of X to Er is modified by a fractionation factor (f_{11}), as described in eq 1.

$$X \xrightarrow{f_{11}k_{11}} Er + P \tag{1}$$

where X = Ea + Eb + Ec + Ed + Ee and

$$f_{11} = \frac{Ed}{X} = \frac{Ed}{Ea + Eb + Ec + Ed + Ee} \tag{2}$$

At equilibrium with no net reaction or with a very low value of k_{11} compared to other rate constants inside the box, the ratio of each form can be presented in the form of kinetic constants.

Therefore

$$Ea/Ed = \frac{k_2k_6}{k_1k_5[G]},\ Eb/Ed = \frac{k_6}{k_5},$$
$$Ec/Ed = \frac{k_8k_{10}}{k_7k_9},\ Ee/Ed = \frac{k_{10}}{k_9}$$

Substitution of the rate constant ratios specified above into eq 2 yields eq 3.

$$f_{11} = \frac{1}{\frac{k_2k_6}{k_1k_5[G]} + \frac{k_6}{k_5} + \frac{k_8k_{10}}{k_7k_9} + \frac{k_{10}}{k_9} + 1} \tag{3}$$

Rearrangement of eq 3 results in eq 4

$$f_{11} = \frac{1}{\frac{\frac{k_6}{k_5} + \frac{k_8k_{10}}{k_7k_9} + \frac{k_{10}}{k_9} + 1}{\frac{k_2k_6}{k_1k_5[G]} + \frac{k_6}{k_5} + \frac{k_8k_{10}}{k_7k_9} + \frac{k_{10}}{k_9} + 1} + 1} \tag{4}$$

The observed rate constant (k_{obs}) of the reduction step is equal to $k_{11}f_{11}$. Substitution of the factor f_{11} into k_{obs} yields eq 5.

$$k_{obs} = \frac{\frac{k_5k_7k_9k_{11}}{k_5k_7k_9 + k_5k_7k_{10} + k_5k_8k_{10} + k_6k_7k_9}[G]}{\frac{k_2k_6k_7k_9}{k_1(k_5k_7k_9 + k_5k_7k_{10} + k_5k_8k_{10} + k_6k_7k_9)} + [G]} \tag{5}$$

Enzyme-Monitored Turnover Experiments. Steady-state kinetic experiments were performed using the enzyme-monitored turnover method as described by Chance and Gibson (*28*, *29*). Details of the analysis of P2O kinetics were previously described (*14*). The experiments used an excess of glucose over the concentration of oxygen (0.26 mM after mixing), and the reactions were monitored at 452 nm to measure the concentration of the oxidized enzyme after the steady-state period had been reached before all the oxygen had been consumed. The area under the curve is proportional to the amount of oxygen remaining. Initial rates of the reaction at any remaining oxygen concentrations were calculated according to eqs 6 and 7.

$$v = \frac{dA}{dt}\frac{[O_2]_{total}}{A_{total}} \tag{6}$$

$$[O_2] = [O_2]_{total}\frac{A_{t_1 \rightarrow final}}{A_{total}} \tag{7}$$

where dA is the area of each segment that corresponds to a division on the X-axis (dt), $dt = t_2 - t_1$ ($t_2 > t_1$), A_{total} is the total area under the trace, $A_{t_1 \rightarrow final}$ is the area under the trace from t_1 to the end, and $[O_2]_{total}$ equals 0.26 mM. Areas under the curves (linear time) were integrated using Kaleidagraph 4.0. Steady-state kinetic parameters were calculated from fits of the initial rates versus the concentration of oxygen at various glucose concentrations using Enzfitter (BIOSOFT, Cambridge, U.K.) and eq 8 for calculation of k_{cat}, K_m^G, $K_m^{O_2}$.

$$v = \frac{V[G][O_2]}{K_m^G[G] + K_m^{O_2}[O_2] + [G][O_2]} \quad (8)$$

RESULTS

Reduction of H167A by D*-Glucose*. A solution of the oxidized enzyme in 50 mM sodium phosphate buffer (pH 7.0) was mixed with solutions of the same buffer containing various concentrations of D-glucose using a stopped-flow spectrophotometer under anaerobic conditions. Flavin reduction was monitored at 10 nm intervals from 310 to 550 nm. The maximum absorbance changes were observed at 400 and 452 nm, and kinetic traces at these wavelengths were used for the analysis (Figure 1A,B). Kinetic traces show four distinguishable phases with only two or three phases observed at each D-glucose concentration. The approximate time at the end of each kinetic phase is represented by a number, and the letter H is used for the highest D-glucose concentration and L for the lowest concentration. The first phase [0.002−0.036 s (1H) for 50 mM D-glucose and 0.002−0.67 s (1L) for 0.4 mM D-glucose] is represented by an increase in the absorbance at 400 nm (Figure 1A) and a small change at 452 nm (Figure 1B). This phase is interpreted as the formation of a Michaelis complex between the oxidized enzyme and D-glucose, as found in the wild-type enzyme (*14*), and it was detected at all concentrations of D-glucose used. However, the absorbance change after the first phase is different at different D-glucose concentrations. At D-glucose concentrations of 12.8, 25.6, and 50 mM, the second phase [0.036−0.1 s (2H) in Figure 1A] appeared as a small absorbance decrease at 400 nm, consistent with rate constants of ~28 s^{-1}. The second phase was not observed at concentrations of D-glucose lower than 12.8 mM. At D-glucose concentrations of 0.4−3.2 mM, the reactions showed third [~0.3−15 s (3L)] and fourth [~15−120 s (4L)] phases (Figure 1A). These two phases are likely to represent reduction of the FAD cofactor, as they both show large absorbance decreases at 400 and 452 nm (Figure 1A,B). The third phase at D-glucose concentrations of 0.4−1.6 mM accounted for approximately 65% of the total change, whereas the following fourth phase accounted for 35% (Figure 1A). At 3.2 mM D-glucose, the amplitude of the third phase increased to ~85%. When using D-glucose concentrations of 6.4−50 mM, the third and fourth phases merged to form a single homogeneous flavin reduction phase. The amplitude of each kinetic phase does not depend on substrate concentration in the wild-type enzyme (*14*).The data imply that the mutant reaction may be accomplished using two pathways and that the partition of both pathways is dependent on the concentration of D-glucose (see later analysis using kinetic simulations).

The observed rate constants (k_{obs}) of the first phase, as determined using kinetic traces at 400 nm, show a hyperbolic dependence on the concentration of D-glucose, approaching the limiting value (k_{max}) of 133 ± 5 s^{-1} with an intercept value (k_c) of 2 ± 0.8 s^{-1} according to eq 9. This result suggests that the binding of D-glucose to the enzyme involves more than one step. The observed K_d of D-glucose binding (26.5 ± 2 mM) was obtained from the D-glucose concentration that gives half of the value of the saturating rate constant (Figure 2A, eq 9).

$$k_{obs} = \frac{k_{max}[G]}{K_d + [G]} + k_c \quad (9)$$

The second phase (observed rate constant of ~28 s^{-1}) is likely to exist at all concentrations but is masked at lower D-glucose concentrations. Only D-glucose concentrations of 12.8, 25.6, and 50 mM (where the rate constants of the first phase are 46.5, 66.1, and 89.6 s^{-1}, respectively) allow detection of the second phase. At D-glucose concentrations of 0.4, 0.8, 1.6, and 3.2 mM, the observed rate constants for the third phase are 0.13, 0.23, 0.34, and 0.35 s^{-1}, respectively [Figure 2B (○)] and for the fourth phase 0.056, 0.11, 0.17, and 0.21 s^{-1} [Figure 2B (●)], respectively. At D-glucose concentrations of 6.4, 12.8, 25.6, and 50 mM, the third and fourth phases merge to form a single flavin reduction phase and the values of k_{obs} for the flavin reduction are 0.33, 0.37, 0.39, and 0.41 s^{-1}, respectively [Figure 2B (●)]. These rate constants

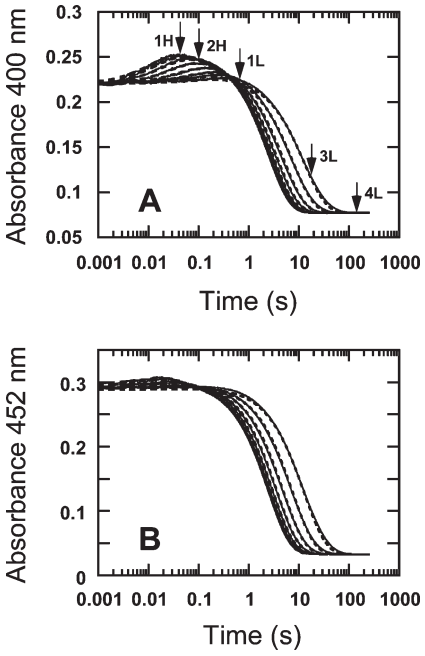

FIGURE 1: Kinetic traces of the reductive half-reaction of H167A with D-glucose. A solution of the enzyme (22 μM) was mixed with solutions of D-glucose at concentrations of 0.4, 0.8, 1.6, 3.2, 6.4, 12.8, 25.6, and 50 mM (from right to left, respectively) in 50 mM sodium phosphate buffer (pH 7.0). All concentrations quoted are those after mixing, and the reactions were performed using the stopped-flow spectrophotometer at 4 °C under anaerobic conditions. The approximate times at the end of the first, second, third, and fourth phases are specified with the corresponding numbers. L designates a D-glucose concentration of 0.4 mM, and H designates a D-glucose concentration of 50 mM. The reactions were monitored at 400 (A) and 452 nm (B). The first-exponential phase is a large absorbance increase at 400 nm, and the traces from bottom to top represent lower to higher concentrations of D-glucose, respectively. The dotted lines represent simulations based on the model presented in Scheme 2 with the kinetic parameters listed in Table 1.

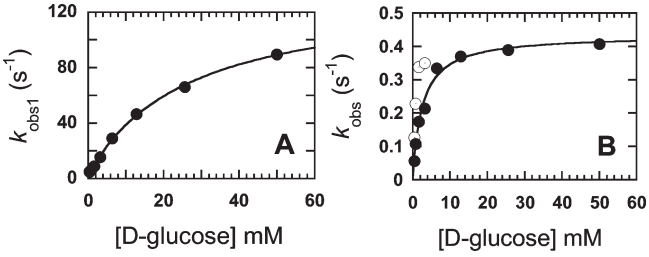

FIGURE 2: (A) Observed rate constants of the first phase (k_{obs}) from the kinetic traces in Figure 1 plotted vs D-glucose concentrations. (B) Observed rate constants of the third (○) and fourth phases (●) were analyzed from the traces in Figure 1 at D-glucose concentrations of 0.4−3.2 mM. At D-glucose concentrations of 6.4−50 mM, the values of k_{obs} of the flavin reduction are plotted as filled circles.

Table 1: Rate Constants Obtained from Kinetic Analysis and Simulations of the Reductive Half-Reactions of H167A with D-Glucose and 2-*d*-D-Glucose

rate constants				extinction coefficient (M^{-1} cm^{-1})	
observed rate and equilibrium constants	calculated apparent rate constants	individual rate constants from simulations	chemical species[a]	400 nm	452 nm
$K^{H}_{obs(Glu)}$ = 2.5 ± 0.3 mM	$K^{H}_{app(Glu)}$ = 2.3 mM	k_1 = 21000 ± 3215 M^{-1} s^{-1}	E_{ox}	9950	13000
$K^{D}_{obs(Glu)}$ = 2.3 ± 0.3 mM	$K^{D}_{app(Glu)}$ = 2.3 mM	k_2 = 2000 ± 321 s^{-1}	E'_{ox}:G	9950	13700
$k^{H}_{obs(reduction)}$ = 0.43 ± 0.01 s^{-1}	$K^{H}_{app(reduction)}$ = 0.44 s^{-1}	k_3 = 38000 ± 3786 M^{-1} s^{-1}	E^{*}_{ox}:G	10000	13700
$k^{D}_{obs(reduction)}$ = 0.11 ± 0.003 s^{-1}	$K^{D}_{app(reduction)}$ = 0.11 s^{-1}	k_4 = 1500 ± 153 s^{-1}	E''_{ox}:G	11450	12700
		k_5 = 130 ± 15 s^{-1}	E^{**}_{ox}:G	11740	14800
		k_6 = 5 ± 1 s^{-1}	Er	3467	1472
		k_7 = 130 ± 12 s^{-1}			
		k_8 = 12 ± 2 s^{-1}			
		k_9 = 20 ± 1 s^{-1}			
		k_{10} = 10 ± 1 s^{-1}			
		k_{11} = 0.7 ± 0.02 s^{-1}			
		k^{H}_{11} (k^{H}_{red}) = 0.7 ± 0.02 s^{-1}			
		k^{D}_{11} (k^{D}_{red}) = 0.17 ± 0.004 s^{-1}			

[a]Rate constants and chemical species are according to the reaction mechanism presented in Scheme 2.

are hyperbolically dependent on the concentrations of D-glucose, approaching the limit of 0.43 ± 0.01 s^{-1} (Table 1 and Figure 2B). The D-glucose concentration giving a half-saturation value is 2.5 ± 0.3 mM. The results from the kinetic analysis described above indicate that the reduction kinetics of H167A is multiphasic and complex, as the substrate concentration can influence the kinetic appearance. To identify the steps involved in the flavin reduction unambiguously and determine whether H167A can oxidize D-glucose at positions other than C2, we investigated the reduction of H167A by 2-*d*-D-glucose, 3-*d*-D-glucose, and 1,2,3,4,5,6,6-d_7-D-glucose.

Primary Kinetic Isotope Effects on the Reductive Half-Reaction of H167A and Regiospecificity of D-Glucose Oxidation. H167A was reduced by 2-*d*-D-glucose in the same fashion as described above for the reduction by D-glucose. The reaction was monitored at 400 and 452 nm (Figure 3A,B). The results show four distinguishable phases that are similar to those observed during the reduction by D-glucose (Figure 1). At all 2-*d*-D-glucose concentrations, the first phase (~0.002−0.036 s) represents an increase in absorbance at 400 nm (Figure 3A), with a slight increase in absorbance at 452 nm (Figure 3B), and this is similar to the first phase observed in the reaction with D-glucose (Figure 1A,B). This indicates that the first phase does not involve cleavage of the D-glucose C2−H bond and confirms its assignment as the formation of an initial enzyme−substrate complex (Figure 1A,B). The following second phase could be detected only when using 2-*d*-D-glucose at 12.8, 25.6, and 50 mM, similar to the case with D-glucose. The following third and fourth phases, as shown by large decreases in absorbance at 400 and 452 nm, respectively, were clearly involved with the flavin reduction and the cleavage of the D-glucose C2−H bond, as their rate constants were significantly affected by 2-*d*-D-glucose. The observed kinetic isotope effect (k^{H}_{obs}/k^{D}_{obs}) is 3.9 ± 0.1 (Table 1). The amplitudes of both phases were also influenced by the concentration of 2-*d*-D-glucose, as was the D-glucose reaction. At 0.8 mM 2-*d*-D-glucose, the amplitude of the fast reduction phase (0.5−23 s) was 53% and the amplitude of the slow phase was 47% (23−200 s). When the substrate concentration was increased, the amplitude of the fast phase also increased. At 3.2 mM 2-*d*-D-glucose, the amplitude of the fast reduction phase was 77% whereas that of the slow phase was 23%. At 6.4−50 mM 2-*d*-D-glucose, the flavin reduction appeared to be homogeneous, as it did for the reaction with

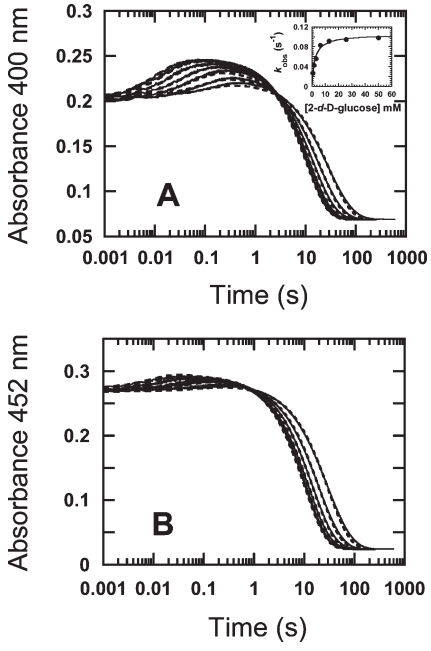

FIGURE 3: Kinetic traces of the reduction of H167A by 2-*d*-D-glucose. A solution of the enzyme (21 μM) was mixed with solutions of 2-*d*-D-glucose at concentrations of 0.8, 1.6, 3.2, 6.4, 12.8, 25.6, and 50 mM (from right to left, respectively) in 50 mM sodium phosphate buffer (pH 7.0). All the concentrations quoted are those after mixing. The reactions were performed using the stopped-flow spectrophotometer at 4 °C under anaerobic conditions. The reactions were monitored at 400 (A) and 452 nm (B). The first exponential phase was a large absorbance increase at 400 nm, and the traces from bottom to top represent lower to higher concentrations of D-glucose, respectively. The dotted lines represent simulations based on the model presented in Scheme 2 with the kinetic parameters listed in Table 1. The inset shows a plot of the k_{obs} of the flavin reduction phase (with a large absorbance decrease at 400 and 452 nm) vs D-glucose concentration.

D-glucose. A plot of the observed rate constants from the fast reduction phase versus the 2-*d*-D-glucose concentrations is hyperbolic. The limiting rate constant is 0.11 ± 0.003 s^{-1}, and the concentration giving a half-saturation value of the rate constant is 2.3 ± 0.3 mM (inset of Figure 3A).

To investigate whether any phase of the reductive half-reaction of H167A is involved with the oxidation of D-glucose at C3 or

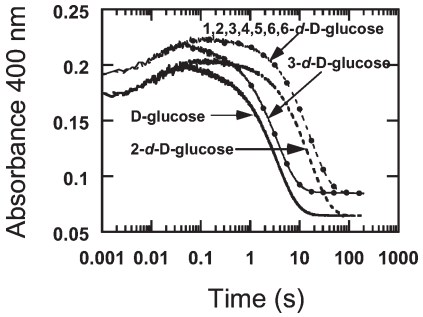

FIGURE 4: Use of kinetic isotope effects to identify the regiospecificity of the sugar oxidation in H167A. A solution of H167A (22 μM) was mixed with solutions of 50 mM D-glucose, 50 mM 2-*d*-D-glucose, 50 mM 3-*d*-D-glucose, and 50 mM 1,2,3,4,5,6,6-d_7-D-glucose. The concentrations quoted represent those after mixing, and the reactions were conducted in a fashion similar to that of the reactions described in the legends of Figures 1 and 3. The kinetic traces shown were monitored at 400 nm. The solid and dotted lines represent the reduction by D-glucose and 2-*d*-D-glucose, respectively. The filled circle solid and dashed lines represent the reduction by 3-*d*-D-glucose and 1,2,3,4,5,6,6-d_7-D-glucose, respectively and the traces were offset by +0.01 for the sake of clarity. The trace of 3-*d*-D-glucose is similar to the trace of D-glucose, whereas the trace of 1,2,3,4,5,6,6-d_7-D-glucose is similar to that of 2-*d*-D-glucose.

other positions, experiments using 3-*d*-D-glucose and 1,2,-3,4,5,6,6-d_7-D-glucose as substrates were performed using the same conditions described in the legends of Figures 1−3. The detection of a primary kinetic isotope effect (KIE) from 3-*d*-D-glucose or 1,2,3,4,5,6,6-d_7-D-glucose (in addition to the KIE from D-glucose C2 oxidation) would indicate oxidation of D-glucose at another position apart from C2. The kinetic traces presented in Figure 4 indicate that the reduction by 50 mM 3-*d*-D-glucose (the solid line with filled circles) is essentially the same as that by 50 mM D-glucose (the solid line trace) and shows no KIE, ruling out the oxidation of D-glucose at position C3 (the 3-*d*-D-glucose and 1,2,3,4,5,6,6-d_7-D-glucose traces were offset for the sake of clarity). The second phase (observed rate constant, ~28 s^{-1}) remained in the reaction with 50 mM 3-*d*-D-glucose, indicating that this phase is not involved with the C3 oxidation. A kinetic trace of the oxidation by 50 mM 1,2,3,4,5,6,6-d_7-D-glucose (the dashed line with filled circles) was essentially the same as the trace for reduction by 2-*d*-D-glucose (the dashed line trace), indicating that the oxidation of D-glucose by this mutant occurs regioselectively only at C2. Taken together, these results clearly indicate that the multiple kinetic phases observed in Figure 1 are intrinsic properties of the C2 oxidation by H167A, rather than the oxidation of D-glucose at multiple positions.

Kinetic Model of the Reductive Half-Reaction of H167A Analyzed by Kinetic Simulations and Derivations. The kinetic data presented in Figures 1−4 can be explained using the model shown in Scheme 2, in which a substrate can bind to the enzyme via two possible pathways. From 14 models employed for the simulations (data not shown), this model is the simplest one that generates simulations agreeing well with the experimental data (Figure 1A,B, solid vs dashed lines). Scheme 2 begins with the binding of D-glucose to the enzyme to form the enzyme−substrate complex, E'_{ox}:G or E^*_{ox}:G. The binding to the E^*_{ox}:G form is faster and tighter, with a K_d of ~39 mM (k_4/k_3), whereas the formation of the E'_{ox}:G complex has a lower affinity, with a K_d of ~95 mM (k_2/k_1). As the observed rate constants of the first phase (the binding phase) are hyperbolically dependent on the substrate concentration (Figure 2A), the data indicate the

Scheme 2: Reductive Half-Reaction of the H167A Mutant

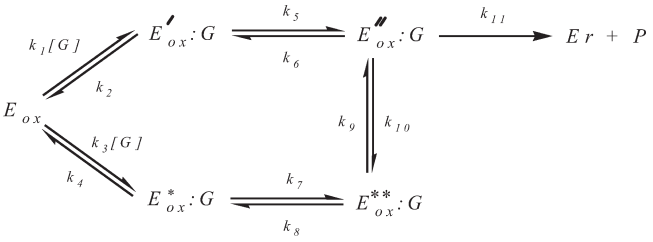

existence of an isomerization step after the initial binding step (Scheme 2). Simulations show that both E'_{ox}:G and E^*_{ox}:G complexes isomerize to the E''_{ox}:G and E^{**}_{ox}:G forms with forward rate constants of 130 ± 15 s^{-1} (k_5 in Scheme 2) and 130 ± 12 s^{-1} (k_7 in Scheme 2), respectively, but with different reverse rate constants of 5 ± 1 s^{-1} (k_6) and 12 ± 2 s^{-1} (k_8), respectively (Scheme 2 and Table 1). An absorbance increase at 400 nm and a small absorbance increase at 452 nm (Figure 1A,B) occurred because of the increase in the molar absorption coefficients upon isomerization (Scheme 2 and Table1).

The observed rate constant of ~28 s^{-1} (detected at D-glucose concentrations of 12.8, 25.6, and 50 mM) is designated as an equilibration step between the E^{**}_{ox}:G and E''_{ox}:G forms as this step was not affected by deuterated D-glucose or D_2O (see the following section). Analysis using simulations yielded a forward rate constant of 20 ± 1 s^{-1} (k_9 in Scheme 2) and a reverse rate constant of 10 ± 1 s^{-1} (k_{10} in Scheme 2). The following step is flavin reduction (k_{11} in Scheme 2) and has a rate constant of 0.7 ± 0.02 s^{-1} (Table 1).

The model in Scheme 2 can explain biphasic flavin reduction at low concentrations of D-glucose. According to this model, D-glucose binds via both pathways. However, at low substrate concentrations, the rate of flavin reduction through the lower pathway (with a lower K_d) is higher than that of the upper pathway. Therefore, biphasic kinetics of flavin reduction was observed at D-glucose concentrations of 0.4−3.2 mM. At high substrate concentrations, both pathways can proceed near their maximum rates and cannot be distinguished kinetically. Hence, flavin reduction appears to be homogeneous at D-glucose concentrations of ≥6.4 mM. In a multistep reaction, observed rate constants of individual steps can be differentiated if an observed rate constant of the preceding step is at least 3-fold greater than that of the following step (*30*). The model in Scheme 2 can also explain why the observed rate constant of 28 s^{-1} can be detected only at high concentrations of D-glucose but not at lower concentrations of D-glucose. According to this model, observed rate constants for the binding of substrate to enzyme plus the first isomerization step in both upper and lower pathways at the saturating concentration of D-glucose ($k_{obs} = k_7 + k_8 = 142\ s^{-1}$, or $k_{obs} = k_5 + k_6 = 135\ s^{-1}$) are much greater than the value of the second isomerization step ($k_{obs} = 28\ s^{-1}$). At lower D-glucose concentrations, these k_{obs} values are not 3-fold greater than the value of the following step, thus masking the detection of a k_{obs} of 28 s^{-1}. Therefore, the model in Scheme 2 can explain why kinetic traces show four distinguishable phases with only two or three phases observed at each D-glucose concentration.

The model in Scheme 2 is also validated by comparison of the experimentally observed rate constants with the calculated apparent rate constants based on the model and the parameters obtained from the simulations (Table 1). The apparent rate constants were calculated on the basis of eq 10 (described in

Materials and Methods) and rate constants from the simulations (Table 1). According to the model in Scheme 2

$$k_{\text{app(reduction)}} = \frac{\dfrac{k_5k_7k_9k_{11}}{k_5k_7k_9 + k_5k_7k_{10} + k_5k_8k_{10} + k_6k_7k_9}[\text{G}]}{\dfrac{k_2k_6k_7k_9}{k_1(k_5k_7k_9 + k_5k_7k_{10} + k_5k_8k_{10} + k_6k_7k_9)} + [\text{G}]} \quad (10)$$

At saturating concentrations of the substrate, [G], $k_{\text{app(reduction)}}$ can be described by eq 11.

$$k_{\text{app(reduction)}} = \frac{k_5k_7k_9k_{11}}{k_5k_7k_9 + k_5k_7k_{10} + k_5k_8k_{10} + k_6k_7k_9} \quad (11)$$

Using eq 11 and individual rate constants from Table 1, we calculated a $k^{\text{H}}_{\text{app(reduction)}}$ of 0.44 s^{-1}. This value agrees well with the experimental value for the observed rate constant [$k^{\text{H}}_{\text{obs}}$ = 0.43 ± 0.013 s^{-1} (Table 1 and Figure 2B)]. Equation 10 also indicates that an apparent concentration of D-glucose giving a half-saturation value [$K_{\text{app(Glu)}}$] can be described, as shown in eq 12:

$$K_{\text{app(Glu)}} = \frac{k_2k_6k_7k_9}{k_1(k_5k_7k_9 + k_5k_7k_{10} + k_5k_8k_{10} + k_6k_7k_9)} \quad (12)$$

Using eq 12 and rate constants from the simulations (Table 1), we calculated a $K^{\text{H}}_{\text{app(Glu)}}$ of 2.3 mM, in good agreement with a $K^{\text{H}}_{\text{obs(Glu)}}$ of 2.5 ± 0.3 mM obtained from the hyperbolic plot (Figure 2B). Therefore, the results in Table 1 confirm that the flavin reduction by D-glucose in H167A occurs according to the model presented in Scheme 2. The results in Table 1 also indicate that the intrinsic reduction rate constant (k^{H}_{11}) is 0.7 ± 0.02 s^{-1}.

Simulations using the model in Scheme 2 were also conducted for the reduction using 2-*d*-D-glucose. We used the same values of the kinetic constants for the simulations as in the D-glucose case, except with a k^{D}_{11} of 0.17 ± 0.004 s^{-1}. Kinetic traces from the simulations agree well with the experimental data (the dashed vs solid lines in Figure 3). According to eq 11, the apparent rate constant of the reduction [$k^{\text{D}}_{\text{app(reduction)}}$] was calculated to be 0.11 s^{-1}, similar to the observed rate constant [$k^{\text{D}}_{\text{obs(reduction)}}$] of 0.11 ± 0.003 s^{-1} obtained from the experiment data (inset of Figure 3A). The value for $K^{\text{D}}_{\text{obs(Glu)}}$ from the hyperbolic plot is 2.3 ± 0.3 mM (data not shown), also similar to the value of 2.3 mM [$K^{\text{D}}_{\text{app(Glu)}}$] calculated from eq 12 and the rate constants listed in Table 1. Therefore, all the comparisons shown in Table 1 indicate good agreement between the calculated and observed values, validating the kinetic model described in Scheme 2.

Solvent Kinetic Isotope Effects on the Reductive Half-Reaction of H167A. Effects of solvent on the reductive half-reaction of H167A were investigated to identify the steps involved in proton transfer. Experiments similar to those in Figures 1 and 3 with 50 mM D-glucose and 50 mM 2-*d*-D-glucose (after mixing) were conducted in D_2O for comparison with the control reaction conducted in H_2O that had gone through the same preparation process (see Materials and Methods). The solid line trace (labeled D-glucose in Figure 5A) shows the reduction of H167A by D-glucose in an H_2O buffer that was monitored using the absorbance change at 400 nm. The observed rate constants for the first, second, and third phases are 90 ± 2, ~28, and 0.43 ± 0.013 s^{-1}, respectively, the same as those shown in Figure 1A,B. This indicates that the solvent exchange process did not interfere with the catalytic reaction. When the reaction with D-glucose was performed in a D_2O buffer, we obtained the dotted line trace

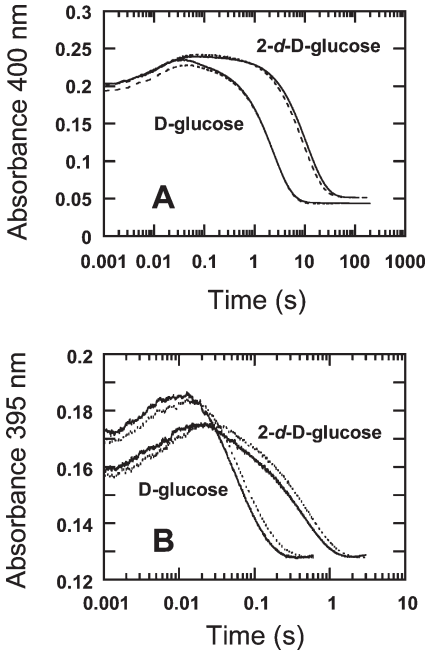

FIGURE 5: Reductive half-reaction of the H167A mutant (A) and wild-type P2O (B) in H_2O and deuteroxide (D_2O) buffer. A solution of H167A or WT (22 μM) was mixed with solutions of 50 mM D-glucose or 50 mM 2-*d*-D-glucose under anaerobic conditions in the stopped-flow spectrophotometer at 4 °C. All the concentrations quoted represent those after mixing. The reactions were performed in 50 mM sodium phosphate buffer in D_2O at pD 7.0 or in H_2O at pH 7.0. The reactions were monitored at 400 and 395 nm. (A) Reaction traces of H167A in H_2O buffer are shown as solid lines, whereas those in D_2O buffer are shown as dotted lines. (B) Reaction traces of WT in H_2O buffer (solid lines) and in D_2O buffer (dotted lines).

labeled D-glucose in Figure 5A. This trace appeared to be the same as the solid line trace of H_2O (Figure 5A) and of the previous section (Figure 1A). The observed rate constants for the first, second, and third phases are 90 ± 2, ~28, and 0.42 ± 0.013 s^{-1}, respectively. These results do not indicate any solvent kinetic isotope effect in the reductive half-reaction of H167A, indicating that the C2 deprotonation of D-glucose is not the main factor limiting any kinetic steps detected by transient kinetics. The dotted line trace of the reduction of H167A by 50 mM 2-*d*-D-glucose in D_2O and the solid line trace of the reduction of H167A by 50 mM 2-*d*-D-glucose in H_2O (Figure 5A) also show no difference in kinetics when superimposed, again indicating no solvent isotope effect. These results suggest that the hydride transfer is decoupled from the C2 deprotonation of D-glucose, as no solvent kinetic isotope effect was detected during the flavin reduction phase. This implies that the mechanism of flavin reduction may be stepwise and preceded by the C2 deprotonation to form an alkoxide intermediate. However, the C2 deprotonation of D-glucose to form the alkoxide intermediate could not be assigned to the first and second phases, as these steps also lack a solvent KIE. The data may be interpreted as the rapid formation of a D-glucose alkoxide once bound to P2O, preceding the kinetics detected using the stopped-flow experiments.

Solvent Kinetic Isotope Effects on the Reductive Half-Reaction of the Wild-Type Enzyme. To confirm that the results presented in the previous section are not artifacts arising from the lack of a flavin covalent linkage, we conducted reactions of the wild-type enzyme in D_2O in the same fashion as those for H167A. The solid line trace that is labeled D-glucose in Figure 5B depicts the reduction of WT by 50 mM D-glucose in

H_2O. This trace exhibits biphasic kinetics with an absorbance increase at 395 nm for the first phase (substrate binding) with a rate constant of 80 ± 5 s^{-1} and a large absorbance decrease for the second phase (16 ± 1 s^{-1}) of flavin reduction. These results are the same as those reported previously (*14*). The reduction of the wild-type enzyme by 50 mM D-glucose in D_2O buffer (the dotted line trace labeled D-glucose in Figure 5B) yielded a kinetic trace that is very similar to that of the reaction in H_2O: the first and the second observed rate constants were 80 ± 7 and 14 ± 1 s^{-1}, respectively. These data indicate no solvent kinetic isotope effect (SKIE) on the first phase and a SKIE of 1.1 ± 0.1 for the second phase of the reductive half-reaction. When we reduced the wild-type enzyme using 50 mM 2-*d*-D-glucose in D_2O buffer (the dotted line trace labeled 2-*d*-D-glucose in Figure 5B), the kinetic trace exhibited biphasic kinetics with an absorbance increase at 395 nm for the first phase of substrate binding (181 ± 5 s^{-1}) and a large absorbance decrease for the second phase (1.9 ± 0.1 s^{-1}) of flavin reduction. The reduction using 50 mM 2-*d*-D-glucose in H_2O buffer (the solid line trace in Figure 5B) shows observed rate constants for substrate binding (181 ± 5 s^{-1}) and flavin reduction (2.3 ± 0.1 s^{-1}) steps similar to those observed for the reaction in D_2O. Therefore, the WT results also show no significant solvent isotope effect when using D-glucose (SKIE for k_{red} of 1.1 ± 0.1) or 2-*d*-D-glucose (SKIE for k_{red} of 0.83 ± 0.04) as substrates, again implying that the C2−OH bond cleavage of D-glucose is not the limiting factor in the reductive half-reaction of P2O.

Oxidative Half-Reaction of H167A. Reduced H167A was prepared as described in Materials and Methods and mixed with buffers containing various concentrations of oxygen. Traces monitored at several wavelengths from 310 to 550 nm exhibited similar kinetics (Figure 6A,B). Large amplitude changes were detected at 335 and 452 nm. Traces at 335 nm (solid lines, Figure 6A) show biphasic kinetics at all oxygen concentrations. At an oxygen concentration of 0.96 mM, the first phase (0.002−0.028 s, the increase in absorbance) indicates the formation of a C4a-hydroperoxyflavin intermediate that subsequently decays in the second phase (0.028−0.4 s) to yield H_2O_2 and the oxidized enzyme, as for WT (*15*). The observed rate constants for the first phase are linearly dependent on the oxygen concentration, with a slope of (4.2 ± 0.2) × 10^4 M^{-1} s^{-1} and an intercept of 19.4 s^{-1} (see the inset of Figure 6A). Both values are similar to those of the wild-type enzyme [(4.3 ± 0.4) × 10^4 M^{-1} s^{-1} and 18 s^{-1}, respectively (*15*)]. The observed rate constants for the second phase (a decrease in absorbance at 335 nm that occurred simultaneously with an absorbance increase at 452 nm) are hyperbolically dependent on the concentration of oxygen (see the inset of Figure 6B). The plot shows a limiting rate constant of 25 ± 3 s^{-1} (Figure 6B), similar to the value of 21 ± 2 s^{-1} observed for WT (*15*).

Kinetic simulations that were conducted in accordance with the two-step consecutive model shown in the dotted line traces agree very well with the experimental data (Figure 6A,B). An analysis based on kinetic simulations yielded a bimolecular rate constant of 7.5 × 10^4 M^{-1} s^{-1} and a reverse rate constant of 2 s^{-1} for the formation of C4a-hydroperoxyflavin. The intermediate subsequently decayed to yield H_2O_2 with a rate constant of 25 ± 3 s^{-1} (Scheme 3). The kinetic parameters of the oxidative half-reaction of H167A are very similar to those of the wild-type enzyme (Table 2).

The absorption characteristics of the C4a-hydroperoxyflavin were calculated using stopped-flow data obtained with the

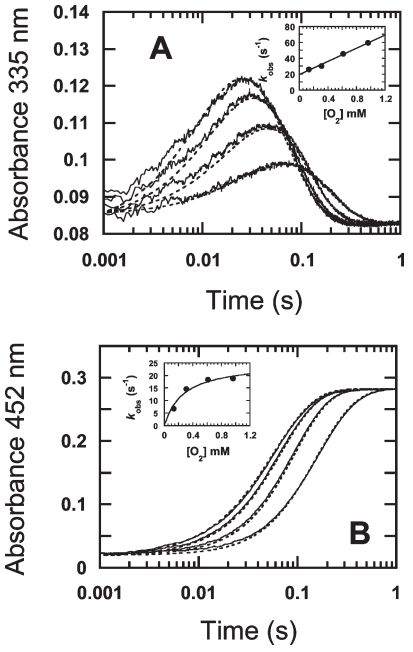

FIGURE 6: Oxidative half-reaction of the H167A mutant. A solution of the reduced enzyme (22 μM) was mixed with the buffer containing 0.13, 0.31, 0.61, and 0.96 mM oxygen in the stopped-flow spectrophotometer at 4 °C. Reactions from low to high concentrations of oxygen are shown from the bottom to top, respectively, at 335 nm and from right to left, respectively, at 452 nm. All the concentrations quoted represent those after mixing. The reactions were performed in 50 mM sodium phosphate buffer (pH 7.0) and were monitored at 335 (A) and 452 nm (B). Both wavelengths show similar kinetics with two exponential phases. The absorbance change at 335 nm increases during the first phase and decreases during the second phase. The data indicate the formation and decay of C4a-hydroperoxyflavin. The inset in panel A shows a plot of the observed rate constants (k_{obs}) of the first phase vs oxygen concentration. The absorbance change at 452 nm indicates a lag during the first phase and a large absorbance increase in the second phase. The inset in panel B shows a plot of k_{obs} for the second phase vs oxygen concentration. The dotted line traces show kinetic simulations based on the model presented in Scheme 3 and the kinetic parameters listed in Table 2.

Scheme 3: Oxidative Half-Reaction of the H167A Mutant

$$E_r + O_2 \underset{k_{13}}{\overset{k_{12}}{\rightleftharpoons}} E\text{-}C(4a)\text{-}OOH \xrightarrow{k_{14}} E_{ox} + H_2O_2$$

reduced enzyme (24.4 μM) reacting with the highest oxygen concentration of 0.96 mM. The reaction was monitored at 5 nm intervals in the 310−550 nm region. Formation of the intermediate was detected maximally at 0.026 s. According to the kinetic parameters described above, the concentrations of each species at 0.026 s were 4.43 μM for the reduced enzyme, 14.8 μM for the C4a-hydroperoxyflavin intermediate, and 5.21 μM for the oxidized enzyme. These values were used for the calculation of absorption spectra of the reduced and oxidized enzymes at the specified concentrations, allowing calculation of the C4a-hydroperoxyflavin intermediate spectrum at 14.8 μM (the spectrum indicated using empty circles in Figure 7). The spectrum was multiplied by a factor of 1.58 to obtain the intermediate spectrum equivalent to 24.4 μM (the spectrum indicated using filled circles in Figure 7). The C4a-hydroperoxyflavin intermediate detected in the reaction of H167A is slightly different compared to that of the WT (the filled circles vs the thick dotted line spectra in Figure 7).

Table 2: Kinetic and Simulation Parameters for the Oxidative Half-Reaction of H167A Compared to Those of the Wild-Type Enzyme

rate constants			extinction coefficient (M^{-1} cm^{-1})	
observed rate constants	rate constants from simulations	chemical species	335 nm	452 nm
$(4.2 \pm 0.2) \times 10^4$ M^{-1} s^{-1}	$k_{12} = 7.5 \times 10^4$ M^{-1} s^{-1}	E_{red}	3890	990
$(4.3 \pm 0.4) \times 10^4$ M^{-1} s^{-1a}	$k_{12} = 5.8 \times 10^4$ M^{-1} s^{-1a}			
–	$k_{13} = 2$ s^{-1}	E-C4a-OOH	6650	3200
–	$k_{13} = 2$ s^{-1a}			
25 ± 3 s^{-1}	$k_{14} = 19$ s^{-1}	E_{ox}	3749	12900
21 ± 2 s^{-1a}	$k_{14} = 18$ s^{-1a}			

[a]Rate constants are from the oxidative half-reaction of wild-type P2O (*15*).

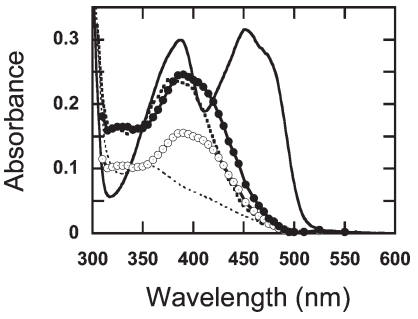

FIGURE 7: Absorption spectrum of the C4a-hydroperoxyflavin intermediate detected during the oxidative half-reaction of H167A. An experiment similar to that shown in Figure 5 was conducted with 0.96 mM oxygen after mixing. The reaction was monitored every 5 or 10 nm between 310 and 550 nm. Kinetic traces measured at individual wavelengths were used to calculate the intermediate spectrum. The empty circle spectrum is that of the C4a-hydroperoxyflavin of H167A (14.8 μM), and it was obtained after subtraction of the absorbance of the reduced enzyme (4.43 μM) and the oxidized enzyme (5.21 μM). The spectrum was multiplied by a factor of 1.58, resulting in the spectrum shown using filled circles, representing the spectrum of the intermediates at 24.4 μM. The bottom dotted line spectrum shows the starting species of the reduced enzyme, whereas the solid line spectrum shows the final species of the oxidized enzyme. The thick dotted line spectrum shows the spectrum of the C4a-hydroperoxyflavin of the wild-type enzyme (22 μM) (*15*).

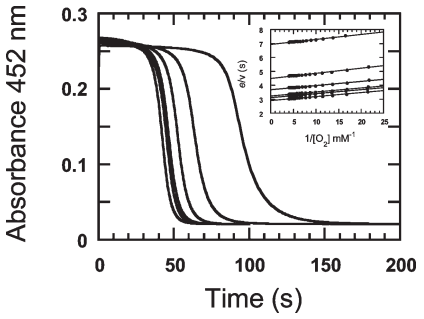

FIGURE 8: Enzyme-monitored turnover experiments. A solution of the H167A mutant (19.2 uM) in 50 mM sodium phosphate buffer (pH 7.0) was mixed with 1, 2, 4, 8, 16, and 30 mM D-glucose (from the right to left, respectively) under air saturation (0.26 mM oxygen) in the stopped-flow spectrophotometer at 4 °C. All the concentrations quoted represent those after mixing. The reaction was monitored at 452 nm. The inset shows a double-reciprocal plot of the initial rates vs oxygen concentration, indicating parallel lines representing the ping-pong mechanism. All steady-state kinetic parameters are listed in Table 3.

In H167A, the intermediate spectral peak is at 388 nm, whereas the WT peak is at 375 nm.

Steady-State Kinetics. We studied the steady-state kinetics of H167A with D-glucose and oxygen as substrates using an enzyme-monitored turnover assay. A solution of the oxidized enzyme (19.2 μM) in air-saturated buffer was mixed with buffers containing various concentrations of D-glucose and 0.26 mM oxygen using the stopped-flow spectrophotometer (the concentrations refer to those present after mixing). The change in flavin absorption was monitored at 452 nm. Figure 8 shows a slow decrease in absorbance at 452 nm, indicating that most of the enzyme population was in the oxidized form during the steady-state period and that the rate of flavin reduction was much slower than that of flavin oxidation. Kinetic traces monitored at 452 nm from low to high concentrations of D-glucose [2, 4, 8, 16, and 30 mM (from right to left, respectively, in Figure 8)] were analyzed as a function of oxygen concentration according to the method of Gibson et al. (*14*, *29*). A primary plot (inset of Figure 8) shows a set of parallel lines that, according to Dalziel's equation in eq 13 (*31*), are consistent with a ping-pong mechanism, which is the case in WT. The steady-state kinetic parameters were analyzed according to eq 8 and are summarized in Table 3.

Steady-state kinetic parameters can also be calculated from the individual rate constants obtained from transient kinetics. On the basis of the net rate method of Cleland (*32*) with modifications according to the rapid equilibrium assumption by Cha (*27*) (Scheme 1), the initial rate equation can be described in terms of the individual rate constants, K_m^G, $K_m^{O_2}$, and k_{cat}, according to eqs 13−17.

Table 3: Correlations of Kinetic Parameters from Steady-State Kinetics and Pre-Steady-State Kinetics

kinetic parameter	experimentally obtained from steady-state kinetics	calculated from pre-steady-state kinetics[a]
K_m^G (mM)	1.5 ± 0.1	2.26
$K_m^{O_2}$ (μM)	21 ± 2	6.36
k_{cat} (s^{-1})	0.39 ± 0.020	0.43

[a]Kinetic parameters were calculated according to eqs 13−17.

$$\frac{e}{v} = \frac{\phi_G}{[G]} + \frac{\phi_{O_2}}{[O_2]} + \phi_0 \tag{13}$$

$$\frac{e}{v} = \frac{k_2 k_6}{k_1 k_5 k_{11}} \frac{1}{[G]} + \frac{k_{13} + k_{14}}{k_{12} k_{14}} \frac{1}{[O_2]} + \frac{k_5 k_7 k_9 + k_5 k_7 k_{10} + k_5 k_8 k_{10} + k_6 k_7 k_9}{k_5 k_7 k_9 k_{11}} + \frac{1}{k_{14}} \tag{14}$$

$$K_m^G = \frac{\phi_G}{\phi_0} \tag{15}$$

$$K_m^{O_2} = \frac{\phi_{O_2}}{\phi_0} \tag{16}$$

$$k_{cat}(\phi_0^{-1}) = \left(\frac{k_5k_7k_9 + k_5k_7k_{10} + k_5k_8k_{10} + k_6k_7k_9}{k_5k_7k_9k_{11}} + \frac{1}{k_{14}}\right)^{-1} \quad (17)$$

Analysis of steady-state kinetics data (Figure 8) according to eq 8 (Materials and Methods) yielded a turnover number (k_{cat}) of 0.39 ± 0.02 s^{-1}, a K_m^G for D-glucose of 1.5 ± 0.1 mM, and a $K_m^{O_2}$ for molecular oxygen of 21 ± 2 μM. Calculation of k_{cat} using eq 17 and the individual rate constants in Table 1 yielded a k_{cat} of 0.43 s^{-1}, which agreed well with the value (0.39 ± 0.02 s^{-1}) obtained from the steady-state kinetics experiments (Table 3). This result also indicates that the reduction step ($k_{11} = 0.7 \pm 0.02$ s^{-1}) is the rate-limiting step of the overall catalytic reaction of H167A. Calculation of K_m^G using eq 15 yielded a value of 2.26 mM, in the same range as the value of 1.5 ± 0.1 mM obtained experimentally (Table 3). The values of $K_m^{O_2}$ obtained from steady-state and transient kinetics are quite different. However, $K_m^{O_2}$ could not be accurately determined from steady-state kinetics, as the oxygen concentration in the $K_m^{O_2}$ range is almost at the end point of the enzyme-monitored turnover experiments. Nevertheless, the excellent agreement between the values of k_{cat} and K_m^G obtained from steady-state kinetics and the value calculated according to Scheme 2 validates the proposed model, as do the kinetic simulations shown in Figures 1, 3, and 6 and reported in Tables 1−3.

DISCUSSION

Our studies of the noncovalent flavin mutant protein, H167A, using transient and steady-state kinetics and kinetic isotope effects have shown that the flavin linkage is mainly important for the reductive half-reaction and that the reduction mechanism of P2O is stepwise. D-Glucose binds to H167A using a multistep binding mode prior to flavin reduction. Our data have also shown that D-glucose is oxidized regiospecifically at C2. A flavinylation linkage is not ubiquitous in flavoenzymes and is thought to help increase the flavin redox potential, which is beneficial for catalysis (*4*, *33*). In P2O, upon removal of the covalent linkage, the redox potential value of FAD decreases from −105 mV in WT to −150 mV in H167A (*23*) and results in ~22-fold slower flavin reduction in H167A than in WT (Figure 1A,B and Table 1). This indicates that the decrease in redox potential is not the primary contributor to the effects of the mutation.

Binding of D-glucose to H167A increases the absorbance at 400 nm (Figures 1 and 3) in a manner similar to that seen when D-glucose and D-galactose bind to WT and Thr169 mutants (*14*, *18*). However, the binding kinetics in H167A is more complicated than in WT and T169 mutants, as shown in Scheme 2. D-Glucose binds to the enzyme via two binding pathways, one with a higher rate and affinity [K_d (k_4/k_3) ~ 39.5 mM] and the other with a K_d (k_2/k_1) of ~95 mM (Scheme 2 and Table 1). Both binding pathways merge to form a single enzyme−substrate complex (E''_{ox}:G) that can be reduced by D-glucose (Scheme 2). We can envisage that the multiple binding steps shown in Scheme 2 may account for all possible modes of binding of D-glucose to the enzyme prior to flavin reduction. As only one active Michaelis complex can undergo the reduction process, all forms must interconvert to form E''_{ox}:G. The nature of these multiple binding steps of D-glucose based on the current data is unclear. It may arise from the binding of D-glucose in the C3 mode prior to equilibration into the C2 mode, or it may be involved with epimerization of the sugar. However, because the space of the D-glucose binding site is rather limited and the crystal structure of the H167A−2FG complex shows that only the β-configuration of D-glucose is bound in H167A (*23*), the involvement of sugar epimerization in the binding process is unlikely.

Using 2-*d*-D-glucose as a substrate in the reaction of H167A, no significant kinetic isotope effect was observed for the D-glucose binding step, unlike that observed for WT. In WT, an inverse kinetic isotope effect was detected at this step (*14*), implying that the C2−H bond is more rigid in the P2O−D-glucose complex than in free D-glucose (*34*, *35*). This indicates that the increased bond constraint at the C2−H bond of D-glucose could not be detected in the H167A−D-glucose complex. We propose that this difference may arise as a result of the greater dynamics and flexibility of the noncovalent FAD cofactor in the active site of H167A, causing no constraint of D-glucose upon binding. A comparison of the H167A and WT X-ray structures has revealed a slight difference in the position of the flavin ring upon removal of the covalent histidyl−FAD linkage (*23*). In WT, the covalent bond between His167 and FAD C8α causes the dimethylbenzenoid ring to be 0.4−0.5 Å closer to the monosaccharide binding site than the flavin ring in the structure of H167A (*10*, *23*). Therefore, the noncovalent FAD in H167A may allow multiple modes of binding of D-glucose (as discussed above), thus alleviating the C2−H bond constraint of D-glucose upon binding to the enzyme.

Multiphasic flavin reduction during the reductive half-reaction of H167A arises from two pathways of D-glucose binding, as shown in Scheme 2. At low substrate concentrations (0.4−3.2 mM), D-glucose binds using both pathways, but the net rate of flavin reduction through the lower pathway (with a lower K_d) is higher than that of the upper pathway, resulting in biphasic kinetics of flavin reduction (Figure 1A,B). At high substrate concentrations (≥6.4 mM), both pathways can proceed near their maximum rates and cannot be distinguished kinetically. Hence, the flavin reduction appears to be homogeneous (Figure 1A,B). The reaction of 2-*d*-D-glucose also supports this model, as both flavin reduction phases show the same observed primary kinetic isotope effect of 3.9 ± 0.1 (Figures 1 and 3 and Table 1). Equations 11 and 12 describe how the model in Scheme 2 results in a $k_{app(reduction)}$ of 0.43 ± 0.01 s^{-1} and a $K_{app(Glu)}$ of 2.5 ± 0.3 mM. Kinetic simulations based on this model agree with the experimental data well (the dotted line vs the solid traces in Figures 1 and 3), validating this model and determining the intrinsic reduction rate constant (k_{11} in Scheme 2) to be 0.7 ± 0.02 s^{-1} (Figure 1A,B and Table 1). When other enzymes in the same GMC oxidoreductase family were mutated at similar residues forming the flavin covalent linkage, mixed reduction kinetics were not observed. In the H99N mutant of choline oxidase, the flavin reduction was ~45-fold slower than for the wild-type enzyme (*36*). The rate constant of flavin reduction was ~90-fold lower for the H121A mutant of cholesterol oxidase than for the wild-type enzyme (*37*). Roles of the flavin covalent linkage appear to vary among the different flavoenzymes.

Reactions of the H167A mutant of P2O from *T. multicolor* with deuterated D-glucose compounds have shown the primary kinetic isotope effect only at position C2, indicating that the enzyme regiospecifically oxidizes D-glucose only at this position (Figure 4). Therefore, the orientation of 2FG in the C3 oxidation mode in the three-dimensional structure of H167A (and also in one of the WT structures) does not reflect a productive binding of D-glucose, and this may be due to the lack of a C2−OH group in 2FG to interact with the catalytic residues, His548 and

Asn593 (*23*). It also implies that the C2−OH group of D-glucose is crucial for the correct alignment of the substrate for C2 oxidation. It has been shown that P2O from *T. multicolor* oxidizes a broad range of sugar substrates regiospecifically at the C2 position, including D-glucose, D-xylose, and L-sorbose (good substrates), and D-galactose and L-arabinose (poor substrates) (*38*). However, oxidation at C3 was reported as a side reaction of P2O from *Pinguicula gigantean* when 2-deoxy-D-glucose, methyl β-D-glucosides, and methyl β-D-galactosides were used as substrates (*11*, *39*). As the X-ray structure of P2O from *P. gigantean* has not been reported, no specific comments regarding the structural differences between the P2Os of these two species are possible at this time.

Pre-steady-state and steady-state kinetics have shown that hydride transfer is the rate-limiting step of the overall reaction of H167A. The k_{red} of the mutant is 0.7 ± 0.02 s^{-1}, which is ~22-fold slower than that of WT, at 15.3 s^{-1} (*14*). In the WT reaction, the overall turnover is controlled by the flavin reduction and C4a-hydroperoxyflavin decay steps (*14*). In addition, the results presented in Figure 5 indicate no solvent kinetic isotope effect, implying that the deprotonation of the C2−OH group from D-glucose does not limit any steps in the reductive half-reaction. Substrate dehydrogenation by flavoenzymes (*20*), including methanol oxidase (*40*), amino acid oxidase (*19*), amine oxidase (*41*), flavocytochrome b_2 (*42*, *43*), glucose oxidase (*29*, *44*), choline oxidase (*21*, *22*), cholesterol oxidase (*45*), and cellobiose dehydrogenase (*46*), have been actively investigated over the past two decades. The mechanisms of most of these enzymes have been shown to be consistent with the hydride transfer mechanism (*19*). According to the hydride transfer mechanism, an active site base in P2O (His548) must abstract the proton of the C2−OH group, forming a D-glucose alkoxide intermediate, before the transfer of a hydride equivalent from the C2−H group to flavin N5 (Figure 9). When the reaction is conducted in D_2O, the deprotonation step of the C2−OD group should have a slower rate constant than the deprotonation step of the C2−OH group. The fact that no solvent kinetic isotope effect was detected suggests that the deprotonation of the C2−OH bond is not synchronized with the hydride transfer from the C2−H bond and does not limit any steps during the reductive half-reaction. It also implies that D-glucose may readily form an alkoxide intermediate once it is bound to P2O to facilitate the transfer of a hydride equivalent to flavin N5 (Figure 9).

The kinetic isotope effects on the reductive half-reaction of P2O are similar to those of choline oxidase (*21*), where the removal of protons from the reactive hydroxyl group of choline is proposed to be facilitated by the preorganization of the environment of the residues at the active site to allow the formation of the alkoxide intermediate (*22*, *47*). Similarly, no solvent isotope effect was detected in the V/K of glucose oxidase (*48*) or D-amino acid oxidase (*49*, *50*). Solvent and primary kinetic isotope effects were also used to probe the relative timing of lactate O−H and C−H bond cleavage in the enzyme flavocytochrome b_2 (*51*). Direct measurement of flavin reduction by deuterated lactate using stopped-flow experiments indicates a $^{D}k_{red}$ of 5.4, whereas the experiments conducted in D_2O show a $^{D_2O}k_{red}$ of 1.0. These data were later interpreted to indicate a stepwise hydride transfer mechanism (*42*). In manitol dehydrogenase, a solvent isotope effect was not detected during the burst kinetic phase of NAD^+ reduction but was found during the steady-state turnovers (*52*). These results indicate that the manitol C−OH bond is cleaved

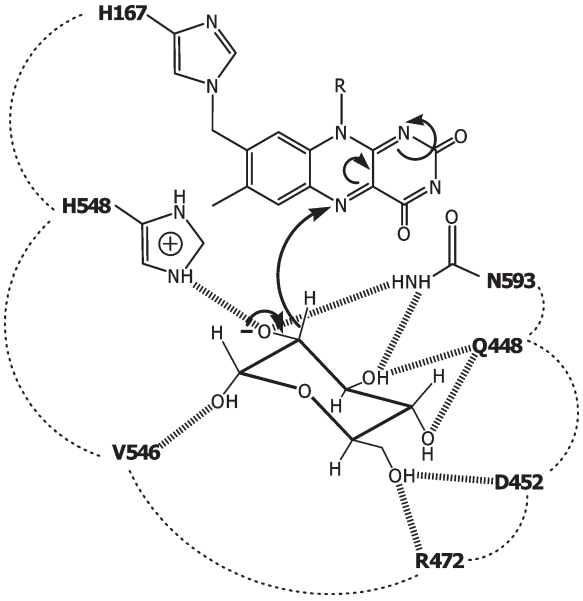

FIGURE 9: Reaction mechanism of P2O from *T. multicolor* that is currently consistent with the stepwise hydride transfer mechanism. Interactions between D-glucose and the active site residues are based on ref *23*.

prior to the hydride transfer step and that the solvent kinetic isotope effect during turnover is due to NADH release (*52*). These interpretations are similar to those of the P2O data reported here, in that formation of the D-glucose alkoxide intermediate may occur before the hydride transfer step.

Although the FAD covalent linkage with His167 is important for the reductive half-reaction, it is clearly not involved in the oxidative half-reaction of P2O. The kinetic constants ($k_{12} = 7.5 \times 10^4$ M^{-1} s^{-1}, $k_{13} = 2$ s^{-1}, and $k_{14} = 19$ s^{-1} in Table 2) and absorption characteristics of the C4a-hydroperoxyflavin intermediate in the mutant are similar to those of WT (Figure 7). In noncovalent flavin mutants of enzymes in the GMC oxidoreductase superfamily, the kinetic parameters of the oxidative half-reaction were not significantly affected. The k_{cat}/K_{oxygen} of the H99N mutant of choline oxidase is 12.4×10^4 M^{-1} s^{-1}, whereas that of the wild-type enzyme is 8.6×10^4 M^{-1} s^{-1} (*21*, *36*). In the H121A mutant of cholesterol oxidase (from *Brevibacterium sterolicum*), the rate constant for flavin oxidation is approximately half that of the wild type (*37*). Enhanced-statistics molecular dynamics simulations have shown that in a flavin monooxygenase (C_2), multiple diffusion pathways are employed to absorb and converge oxygen molecules to a hydrophobic pocket near the flavin C4a atom, forming the C4a-hydroperoxyflavin intermediate (*53*, *54*). In P2O, it has been proposed that the active site hydrophobic pocket that results from the closed loop conformation (*15*, *23*) may accommodate a peroxide group at the flavin C4a position (*15*). Therefore, the removal of a flavin covalent linkage in H167A (which is far from the flavin C4a position) did not affect the stability of the C4a-hydroperoxyflavin (Figure 7). This clearly shows that the covalent linkage is not a factor that enables P2O to form the C4a-hydroperoxyflavin. On the contrary, residue changes around the active site (such as mutations of Thr169 located around the flavin N5 region) resulted in the abolishment of intermediate formation (*18*).

In summary, the studies of the H167A mutant of P2O presented here provide insights into the reaction mechanisms of P2O. The FAD covalent linkage through His167 is important mainly for the reductive half-reaction, as the flavin reduction rate

decreased ~22-fold and the mode of D-glucose binding was more complex in the mutant. Studies of D-glucose variants deuterated at various positions indicate that the enzyme oxidizes D-glucose regiospecifically at C2. On the basis of the solvent kinetic isotope effects on the reductive half-reaction of the wild-type and mutant enzymes, it appears that the deprotonation of the C2−OH group of D-glucose is not synchronized with the cleavage of the D-glucose C2−H bond and may readily occur upon the binding of D-glucose as an alkoxide form.

ACKNOWLEDGMENT

We thank Warintra Pitsawong for critical reading of the manuscript.

REFERENCES

1. Fraaije, M. W., Sjollema, K. A., Veenhuis, M., and van Berkel, W. J. (1998) Subcellular localization of vanillyl-alcohol oxidase in *Penicillium simplicissimum*. *FEBS Lett. 422*, 65–68.
2. Leferink, N. G., Heuts, D. P., Fraaije, M. W., and van Berkel, W. J. (2008) The growing VAO flavoprotein family. *Arch. Biochem. Biophys. 474*, 292–301.
3. van Hellemond, E. W., Leferink, N. G., Heuts, D. P., Fraaije, M. W., and van Berkel, W. J. (2006) Occurrence and biocatalytic potential of carbohydrate oxidases. *Adv. Appl. Microbiol. 60*, 17–54.
4. Heuts, D. P., Scrutton, N. S., McIntire, W. S., and Fraaije, M. W. (2009) What's in a covalent bond? On the role and formation of covalently bound flavin cofactors. *FEBS J. 276*, 3405–3427.
5. Kim, J., Fuller, J. H., Kuusk, V., Cunane, L., Chen, Z. W., Mathews, F. S., and McIntire, W. S. (1995) The cytochrome subunit is necessary for covalent FAD attachment to the flavoprotein subunit of *p*-cresol methylhydroxylase. *J. Biol. Chem. 270*, 31202–31209.
6. Hassan-Abdallah, A., Bruckner, R. C., Zhao, G., and Jorns, M. S. (2005) Biosynthesis of covalently bound flavin: Isolation and in vitro flavinylation of the monomeric sarcosine oxidase apoprotein. *Biochemistry 44*, 6452–6462.
7. Jin, J., Mazon, H., van den Heuvel, R. H., Heck, A. J., Janssen, D. B., and Fraaije, M. W. (2008) Covalent flavinylation of vanillyl-alcohol oxidase is an autocatalytic process. *FEBS J. 275*, 5191–5200.
8. Scrutton, N. S., Packman, L. C., Mathews, F. S., Rohlfs, R. J., and Hille, R. (1994) Assembly of redox centers in the trimethylamine dehydrogenase of bacterium W3A1. Properties of the wild-type enzyme and a C30A mutant expressed from a cloned gene in *Escherichia coli*. *J. Biol. Chem. 269*, 13942–13950.
9. Leitner, C., Volc, J., and Haltrich, D. (2001) Purification and characterization of pyranose oxidase from the white rot fungus *Trametes multicolor*. *Appl. Environ. Microbiol. 67*, 3636–3644.
10. Hallberg, B. M., Leitner, C., Haltrich, D., and Divne, C. (2004) Crystal structure of the 270 kDa homotetrameric lignin-degrading enzyme pyranose 2-oxidase. *J. Mol. Biol. 341*, 781–796.
11. Giffhorn, F. (2000) Fungal pyranose oxidases: Occurrence, properties and biotechnical applications in carbohydrate chemistry. *Appl. Microbiol. Biotechnol. 54*, 727–740.
12. Spadiut, O., Radakovits, K., Pisanelli, I., Salaheddin, C., Yamabhai, M., Tan, T. C., Divne, C., and Haltrich, D. (2009) A thermostable triple mutant of pyranose 2-oxidase from *Trametes multicolor* with improved properties for biotechnological applications. *Biotechnol. J. 4*, 525–534.
13. Halada, P., Leitner, C., Sedmera, P., Haltrich, D., and Volc, J. (2003) Identification of the covalent flavin adenine dinucleotide-binding region in pyranose 2-oxidase from *Trametes multicolor*. *Anal. Biochem. 314*, 235–242.
14. Prongjit, M., Sucharitakul, J., Wongnate, T., Haltrich, D., and Chaiyen, P. (2009) Kinetic mechanism of pyranose 2-oxidase from *Trametes multicolor*. *Biochemistry 48*, 4170–4180.
15. Sucharitakul, J., Prongjit, M., Haltrich, D., and Chaiyen, P. (2008) Detection of a C4a-hydroperoxyflavin intermediate in the reaction of a flavoprotein oxidase. *Biochemistry 47*, 8485–8490.
16. Orville, A. M., Lountos, G. T., Finnegan, S., Gadda, G., and Prabhakar, R. (2009) Crystallographic, spectroscopic, and computational analysis of a flavin C4a-oxygen adduct in choline oxidase. *Biochemistry 48*, 720–728.
17. Mallett, T. C., and Claiborne, A. (1998) Oxygen reactivity of an NADH oxidase C42S mutant: Evidence for a C(4a)-peroxyflavin intermediate and a rate-limiting conformational change. *Biochemistry 37*, 8790–8802.
18. Pitsawong, W., Sucharitakul, J., Prongjit, M., Tan, T. C., Spadiut, O., Haltrich, D., Divne, C., and Chaiyen, P. (2010) A conserved active-site threonine is important for both sugar and flavin oxidations of pyranose 2-oxidase. *J. Biol. Chem. 285*, 9697–9705.
19. Fitzpatrik, P. F. (2004) Carbanion versus hydride transfer mechanisms in flavoprotein-catalyzed dehydrogenations. *Bioorg. Chem. 32*, 125–139.
20. Fitzpatrick, P. F. (2001) Substrate dehydrogenation by flavoproteins. *Acc. Chem. Res. 34*, 299–307.
21. Fan, F., and Gadda, G. (2005) On the catalytic mechanism of choline oxidase. *J. Am. Chem. Soc. 127*, 2067–2074.
22. Gadda, G. (2008) Hydride transfer made easy in the reaction of alcohol oxidation catalyzed by flavin-dependent oxidases. *Biochemistry 47*, 13745–13753.
23. Kujawa, M., Ebner, H., Leitner, C., Hallberg, B. M., Prongjit, M., Sucharitakul, J., Ludwig, R., Rudsander, U., Peterbauer, C., Chaiyen, P., Haltrich, D., and Divne, C. (2006) Structural basis for substrate binding and regioselective oxidation of monosaccharides at C3 by pyranose 2-oxidase. *J. Biol. Chem. 281*, 35104–35115.
24. Danneel, H. J., Rossner, E., Zeeck, A., and Giffhorn, F. (1993) Purification and characterization of a pyranose oxidase from the basidiomycete *Peniophora gigantea* and chemical analyses of its reaction products. *Eur. J. Biochem. 214*, 795–802.
25. Macheroux, P. (1999) UV-Visible Spectroscopy as a Tool to Study Flavoproteins. In Flavoprotein Protocols (Chapman, S. K., and Reid, G. A., Eds.) pp 1−7, Humana Press, Totowa, NJ.
26. Schowen, B. K., and Schowen, R. L. (1982) Solvent isotope effects on enzyme systems. *Methods Enzymol. 87*, 551–660.
27. Cha, S. (1968) A simple method for derivation of rate equations for enzyme-catalyzed reactions under the rapid equilibrium assumption or combined assumptions of equilibrium and steady state. *J. Biol. Chem. 243*, 820–825.
28. Chance, B. (1943) The kinetics of the enzyme-substrate compound of peroxidase. *J. Biol. Chem. 151*, 553–557.
29. Gibson, Q. H., Swoboda, B. E., and Massey, V. (1964) Kinetics and mechanism of action of glucose oxidase. *J. Biol. Chem. 239*, 3927–3934.
30. Hiromi, K. (1979) Analysis of Fast Enzyme Reactions: Transient Kinetics. In Kinetics of Fast Enzyme Reactions, pp 193−194, Kodansha, Ltd. (Halsted Press), Tokyo.
31. Dalziel, K. (1957) Initial steady state velocities in the evaluation of enzyme-coenzyme-substrate reaction mechanisms. *Acta Chem. Scand. 11*, 1706–1723.
32. Cleland, W. W. (1975) Partition analysis and the concept of net rate constants as tools in enzyme kinetics. *Biochemistry 14*, 3220–3224.
33. Efimov, I., and McIntire, W. S. (2004) A study of the spectral and redox properties and covalent flavinylation of the flavoprotein component of *p*-cresol methylhydroxylase reconstituted with FAD analogues. *Biochemistry 43*, 10532–10546.
34. Schramm, V. L. (2007) Binding isotope effects: Boon and bane. *Curr. Opin. Chem. Biol. 11*, 529–536.
35. Cook, P. E., and Cleland, W. W. (2007) Isotope Effects as a Probe of Mechanism. In Enzyme Kinetics and Mechanism (Rogers, R. L., and Scholl, S., Eds.) pp 253−321, Garland Science Publishing, New York.
36. Quaye, O., Cowins, S., and Gadda, G. (2009) Contribution of flavin covalent linkage with histidine 99 to the reaction catalyzed by choline oxidase. *J. Biol. Chem. 284*, 16990–16997.
37. Lim, L., Molla, G., Guinn, N., Ghisla, S., Pollegioni, L., and Vrielink, A. (2006) Structural and kinetic analyses of the H121A mutant of cholesterol oxidase. *Biochem. J. 400*, 13–22.
38. Leitner, C., Haltrich, D., Nidetzky, B., Prillinger, H., and Kulbe, K. D. (1998) Production of a novel pyranose 2-oxidase by basidiomycete *Trametes multicolor*. *Appl. Biochem. Biotechnol. 70−72*, 237–248.
39. Volc, J., Sedmera, P., Havlícek, V., Prikrylová, V., and Daniel, G. (1995) Conversion of D-glucose to D-erythro-hexos-2,3-diulose(2,3-diketo-D-glucose) by enzyme preparations from the basidiomycete *Oudemansiella mucida*. *Carbohydr. Res. 278*, 59–70.
40. Sherry, B., and Abeles, R. H. (1985) Mechanism of action of methanol oxidase, reconstitution of methanol oxidase with 5-deazaflavin, and inactivation of methanol oxidase by cyclopropanol. *Biochemistry 24*, 2594–2605.
41. Scrutton, N. S. (2004) Chemical aspects of amine oxidation by flavoprotein enzymes. *Nat. Prod. Rep. 21*, 722–730.
42. Sobrado, P., and Fitzpatrick, P. F. (2003) Solvent and primary deuterium isotope effects show that lactate CH and OH bond

cleavages are concerted in Y254F flavocytochrome b_2, consistent with a hydride transfer mechanism. *Biochemistry 42*, 15208–15214.
43. Mowat, C. G., Wehenkel, A., Green, A. J., Walkinshaw, M. D., Reid, G. A., and Chapman, S. K. (2004) Altered substrate specificity in flavocytochrome b_2: Structural insights into the mechanism of L-lactate dehydrogenation. *Biochemistry 43*, 9519–9526.
44. Wohlfahrt, G., Witt, S., Hendle, J., Schomburg, D., Kalisz, H. M., and Hecht, H. J. (1999) 1.8 and 1.9 Å resolution structures of the *Penicillium amagasakiense* and *Aspergillus niger* glucose oxidases as a basis for modelling substrate complexes. *Acta Crystallogr. D55* (Part 5), 969–977.
45. Vrielink, A., and Ghisla, S. (2009) Cholesterol oxidase: *Biochemistry* and structural features. *FEBS J. 276*, 6826–6843.
46. Hallberg, B. M., Henriksson, G., Pettersson, G., Vasella, A., and Divne, C. (2003) Mechanism of the reductive half-reaction in cellobiose dehydrogenase. *J. Biol. Chem. 278*, 7160–7166.
47. Fan, F., and Gadda, G. (2007) An internal equilibrium preorganizes the enzyme-substrate complex for hydride tunneling in choline oxidase. *Biochemistry 46*, 6402–6408.
48. Roth, J. P., and Klinman, J. P. (2003) Catalysis of electron transfer during activation of O_2 by the flavoprotein glucose oxidase. *Proc. Natl. Acad. Sci. U.S.A. 100*, 62–67.
49. Denu, J. M., and Fitzpatrick, P. F. (1994) Intrinsic primary, secondary, and solvent kinetic isotope effects on the reductive half-reaction of D-amino acid oxidase: Evidence against a concerted mechanism. *Biochemistry 33*, 4001–4007.
50. Kurtz, K. A., Rishavy, M. A., Cleland, W. W., and Fitzpatrick, P. F. (2000) Nitrogen isotope effects as probes of the mechanism of D-amino acid oxidase. *J. Am. Chem. Soc. 122*, 12896–12897.
51. Sobrado, P., Daubner, S. C., and Fitzpatrick, P. F (2001) Probing the relative timing of hydrogen abstraction steps in the flavocytochrome b_2 reaction with primary and solvent deuterium isotope effects and mutant enzymes. *Biochemistry 40*, 994–1001.
52. Klimacek, M., and Nidetzky, B. (2002) Examining the relative timing of hydrogen abstraction steps during NAD^+-dependent oxidation of secondary alcohols catalyzed by long-chain D-mannitol dehydrogenase from *Pseudomonas fluorescens* using pH and kinetic isotope effects. *Biochemistry 41*, 10158–10165.
53. Baron, R., Riley, C., Chenprakhon, P., Thotsaporn, K., Winter, R. T., Alfieri, A., Forneris, F., van Berkel, W. J., Chaiyen, P., Fraaije, M. W., Mattevi, A., and McCammon, J. A. (2009) Multiple pathways guide oxygen diffusion into flavoenzyme active sites. *Proc. Natl. Acad. Sci. U.S.A. 106*, 10603–10608.
54. Sucharitakul, J., Chaiyen, P., Entsch, B., and Ballou, D. P. (2006) Kinetic mechanisms of the oxygenase from a two-component enzyme, *p*-hydroxyphenylacetate 3-hydroxylase from *Acinetobacter baumannii*. *J. Biol. Chem. 281*, 17044–17053.